IEEE Access
Multidisciplinary | Rapid Review | Open Access Journal

Received 10 April 2023, accepted 9 May 2023, date of publication 16 May 2023, date of current version 24 May 2023.

Digital Object Identifier 10.1109/ACCESS.2023.3276879

RESEARCH ARTICLE

Research on the Output Characteristic of a New Water Hydraulic Electrohydraulic Motor

TONG XING, YING HUANG, CUN GAO, AND JIAN RUAN

Key Laboratory of Special Purpose Equipment and Advanced Manufacturing Technology, Ministry of Education and Zhejiang Province, Zhejiang University of Technology, Hangzhou 310014, China

Corresponding author: Tong Xing (xingtong@zjut.edu.cn)

This work was supported in part by the Natural Science Foundation of China under Grant 51775500, and in part by the National Key Research and Development Program of China under Grant 2019YFB2005204.

ABSTRACT For the hydraulic drilling tool under deep water, an integrated structure of a water hydraulic electrohydraulic motor is proposed, which consists of three parts: pump unit, motor unit, and DC brushless motor. The two-dimensional piston in the pump unit has two degrees of freedom of motion: rotation and reciprocation, so it is compact and can be matched with a high-speed motor to become a high-speed motor pump; the two sets of plungers in the motor unit are balanced with two end-facing cam drive mechanisms to achieve axial force, which is also suitable for high-speed rotation. In this paper, the mechanical structure and working principle of the electrohydraulic motor are described, the mathematical model of the output characteristics of the electrohydraulic motor is established, and the joint simulation model of Adams and AMESim is built, then the relationship between the dynamic characteristics of the electrohydraulic motor and the structure and working parameters is studied. The results show that the higher the speed of the pump unit, the smoother the characteristics of the electrohydraulic motor, when the motor speed is increased from 1000 r/min to 3000 r/min, the pulsation amplitude of the electrohydraulic motor speed is decreased by 200%; the plunger sub of the motor unit should take proper clearance, if the plunger sub clearance is increased to 12 μm, the output speed is decreased by 40% and the leakage volume is increased by 25 times; the motor unit should have proper back pressure to facilitate the smoothness and life of the motor, when the back pressure value is increased from 0.2 MPa to 1.2 MPa, the pressure pulsation at the beginning of the start-up is also greatly reduced.

INDEX TERMS Water hydraulic electrohydraulic motor, integrated design, output characteristics, joint simulation.

I. INTRODUCTION

Underwater construction is best performed with water-hydraulic driven work tools [1], [2], and research into water-hydraulic actuators and motors that do not require pumping stations is the best solution for underwater work tools. In the late 1980s, the United States developed a multifunctional seawater underwater tool system with a pressure of 14 MPa and a flow rate of 45 L/min, including a drill, an impact drill, a rotary disc tool, etc. The drill weighs 6.8 Kg, has a working pressure of 5.2 MPa, and a flow rate of 26.5 L/min [3]. Huazhong University of Science and Technology also developed a similar system of seawater underwater working tools, the weight of its power source is 800 Kg, the power source and working tools are connected by a pressure water pipe, the rated working pressure is 10 MPa, the flow rate is 40 L/min, the whole working system has a complex structure, huge volume and small work to weight ratio [4].

The current smallest size of water hydraulic motor is used a swashplate axial piston structure, there is no compact water hydraulic pump and hydraulic pump motor structure that can be directly driven using tiny motors. Most domestic and foreign scholars have studied the characteristics of hydraulic motors for the traditional swashplate axial plunger structure [5], [6], [7], [8], [9], [10], [11]. Manring studied the

The associate editor coordinating the review of this manuscript and approving it for publication was Atif Iqbal.

torque characteristics of swashplate axial plunger motors and established a single plunger cavity dynamic pressure model mathematical model, analyzed the friction characteristics of the key frictional sub such as plunger sub, and established the corresponding frictional torque model [5], [6]. Kazuyuki and Mitsuei experimentally investigated the effects of key frictional sub of the plunger motor, the flow distribution sub, and their leakage on the motor output torque and speed [7]. Ke et al. established a mathematical model of hydraulic motor efficiency and analyzed the effect of back pressure on its efficiency, and the results showed that the presence of back pressure increased frictional torque [8]. Based on the structural characteristics and operating principle of the double swashplate multi-row axial piston motor, Desheng Wen derived the theoretical instantaneous torque and torque unevenness coefficient of this motor under different operating modes, and analyzed the influence of the internal and external motor torque coefficient ratio on the torque unevenness coefficient, and the results showed that with the increase of the internal and external motor torque coefficient ratio, the torque unevenness coefficient of large torque at low speed is smaller, and the torque instability coefficient of low torque at high speed is larger [9]. Yang et al. simulated the motor output characteristics and studied the effects of parameters such as plunger sub-gap and back pressure on motor speed and output torque, and obtained that smaller gap and back pressure is beneficial to reduce output pulsation, and verified them by experiments [10], [11].

Based on the design principles of two-dimensional hydraulic components [12], [13], [14], [15], an aqueous hydraulic electrohydraulic motor is proposed to integrate a new structure of a two-dimensional piston motor pump with a new structure of an axial plunger motor designed to facilitate the best hydraulic actuator for portable underwater work tools. In the water-hydraulic electrohydraulic motor, an oil-water separation structure is proposed for the pump unit and an axial plunger structure with axial flow distribution is proposed for the motor unit, both of which use an end cam drive mechanism to realize the reciprocating motion of the piston in the pump and the plunger in the motor. Due to the small pressure angle of the driving cams in the pump, the required driving torque is small and can be driven by a micro high-speed motor, thus realizing the integrated electromechanical-hydraulic structure design.

For the technical specifications needed for the underwater hydraulic driller, an integrated structure of a water hydraulic electrohydraulic motor is designed with a continuous output torque of 12.5 Nm, an operating speed of 1000 r/min, and a rated pressure of 10 MPa. In this paper, the mechanical structure and working principle of the hydro-hydraulic electro-hydraulic motor are described, the mathematical model of its output torque and speed is established, its dynamic characteristics utilizing joint hydraulic and dynamics simulation are analyzed, and the influence of parameters such as the speed of the driving motor, the differential pressure between the inlet and outlet of the motor, the plunger gap and back pressure on the output characteristics of the electro-hydraulic motor is analyzed.

II. STRUCTURE AND THEORETICAL ANALYSIS

A. GENERAL STRUCTURE

The structure of the proposed water-hydraulic electrohydraulic motor is shown in Figure 1, which consists of three parts: pump unit, motor unit, and DC brushless motor. The working medium is drawn directly from the external water by filtration, through the pump core part of the single piston, out of the pump unit cylinder window directly into the motor unit cylinder, and then out through the motor unit distribution port.

Figure 2 shows the motor unit structure, with a symmetrical design through shaft structure, through the center hole of the cylinder body; the middle of the motor shaft has a flow distribution groove structure, the motor shaft circumferential uniform distribution of four flow distribution grooves, flow distribution grooves alternately and both sides of the high and low-pressure sink communication, the 2 sink grooves on the motor shaft and the 2 sink grooves on the cylinder body constitute the high and low-pressure cavity of the motor unit; the spline on the outside of the sink groove is installed with a pair of end cams. There are 2 groups of plungers symmetrically distributed in the cylinder block between the two cams, which constitute the axial plunger transmission mechanism with the left and right cams respectively. The plunger assembly consists of rollers, roller holders, and plungers, and there are 8 plunger assemblies in each group, and there is a spring in the bottom chamber of the plungers to press the plungers to the outside and make the rollers contact with the cams; the back of the end cams is supported by 2 thrust bearings.

Figure 3 shows the structure of the pump unit on the left side and the DC motor on the right side. The pump unit adopts a tandem structure, which is the pump core part and the drive part respectively. By double lip skeleton oil seal, the pump core part is separated from the drive part to realize oil and water separation. The pump core part consists of a piston, cylinder body, and 2 sealing rings; 2 sealing rings, cylinder body, and piston form 2 pump chambers on the left and right; 4 grooves are evenly distributed in the circumference of the piston to communicate with the two pump chambers on the left and right in turn, and 4 flow distribution windows are evenly distributed in the circumference of the cylinder body to communicate with the high and low-pressure sink of the pump casing respectively; the driving part is a two-dimensional transmission mechanism composed of a pair of end cams and 4 tapered rollers. The two end cams are connected by the space cup shaft and supported by sliding bearings, the axes of the two pairs of tapered rollers are perpendicular and staggered by a distance of one piston stroke along the rotation axis, and each pair of tapered rollers is in contact with one end cam respectively. The profile curves of

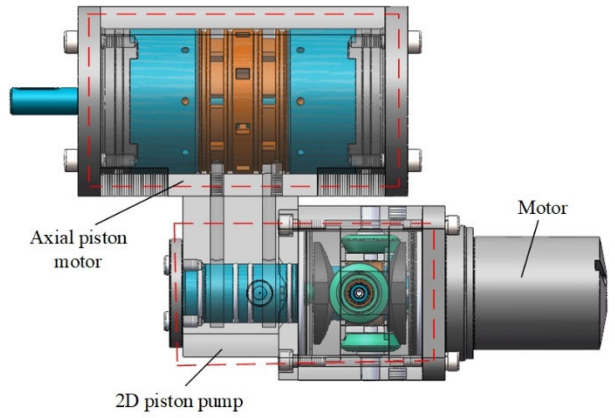

FIGURE 1. Structure of water hydraulic electrohydraulic motor.

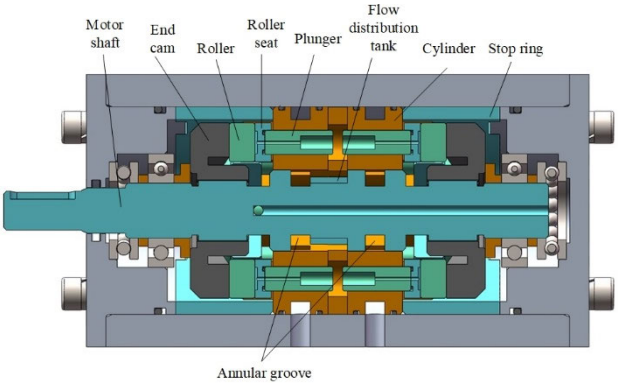

FIGURE 2. Motor unit structure diagram.

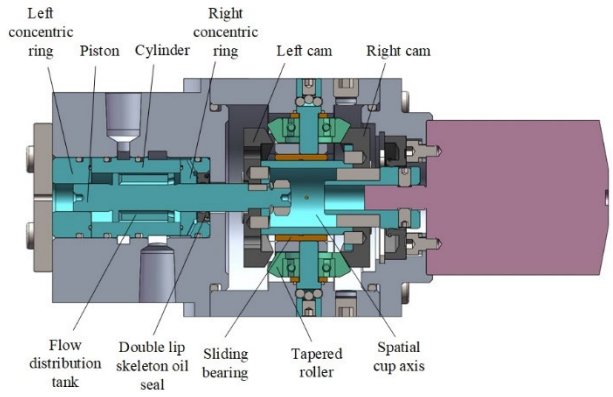

FIGURE 3. Pump unit structure diagram.

the end cams in both the hydraulic pump and the hydraulic motor adopt the law of equal acceleration and deceleration motion.

B. WORKING PRINCIPLES

When working, the motor transmits the rotating motion to the right cam of the pump unit through the coupling, and under the constraint of the two pairs of cone rollers, the pair of end cams rotate and reciprocate at the same time, thus realizing the reciprocating motion of the piston and making the pump cavity volume change periodically, at this time, the two pump cavities communicate with the high and low-pressure ports respectively through the flow grooves on the piston to realize the suction and discharge of the pump. The high-pressure fluid discharged from the pump enters the high-pressure chamber of the motor unit, and through the flow distribution groove on the motor shaft, part of the plunger bottom communicates with the high-pressure chamber, and the rest of the plunger bottom communicates with the low-pressure chamber, and the plunger extends outward under the action of hydraulic pressure so that the plunger acts on the two end cams, which drives the cams to rotate and makes the motor shaft rotate and output mechanical energy.

As shown in Figure 4 for the cross-section of Figure 2, the red marked area indicates the high-pressure area and the blue marked area indicates the low-pressure area. Assuming the initial angle of the motor shaft is 0° as shown in Figure 4 (a), the closed arc section on the motor shaft closes the windows of plunger cavities 1, 3, 5, and 7, and the corresponding plungers 1, 3, 5 and 7 are in the limit position; plunger cavities 2 and 6 are connected with the high-pressure cavity, and the high-pressure fluid enters the bottom of the plunger cavity to push the plungers 2 and 6 out at the moment of zero acceleration, and the cams rotate under the action of the tangential component force; plunger cavity 4 and 8 are connected with the low-pressure cavity, and the fluid in the plunger cavity flows out through the flow distribution window. Figure 4 (b) shows the position of each plunger and cam when the motor shaft turns to 22.5°. Plunger cavities 2, 3, 6, and 7 are connected to the high-pressure cavity, and other plunger cavities are connected to the low-pressure cavity, at this time, plungers 2 and 6 are in the equal deceleration stage, while plungers 3 and 7 are in the equal acceleration stage. Figure 4 (c) shows the position of each plunger and cam when the motor shaft rotates to 45°. The closed arc section on the motor shaft closes the windows of plunger cavities 2, 4, 6, and 8, and the corresponding plungers 2, 4, 6, and 8 are in the limit position; plunger cavities 3 and 7 are connected with the high-pressure cavity, and plungers 3 and 7 are in the moment of zero acceleration, and only plungers 3 and 7 output thrust at this time. As can be seen, the output characteristics of the motor vary with a period of $\pi/4$.

III. MATHEMATIC MODELS

To establish the mathematical model of the output torque of the electrohydraulic motor, firstly the dynamic pressure model of the plunger chamber of its motor unit is established, then the forces on its moving components are analyzed, the force balance equation is established, and finally, the output torque equation of the electrohydraulic motor is obtained. The motion of the electro-hydraulic motor is determined by the motion law of its cam drive mechanism, and the cam shapes of its pump unit and motor unit both adopt equal acceleration and deceleration contour curves, the effect of

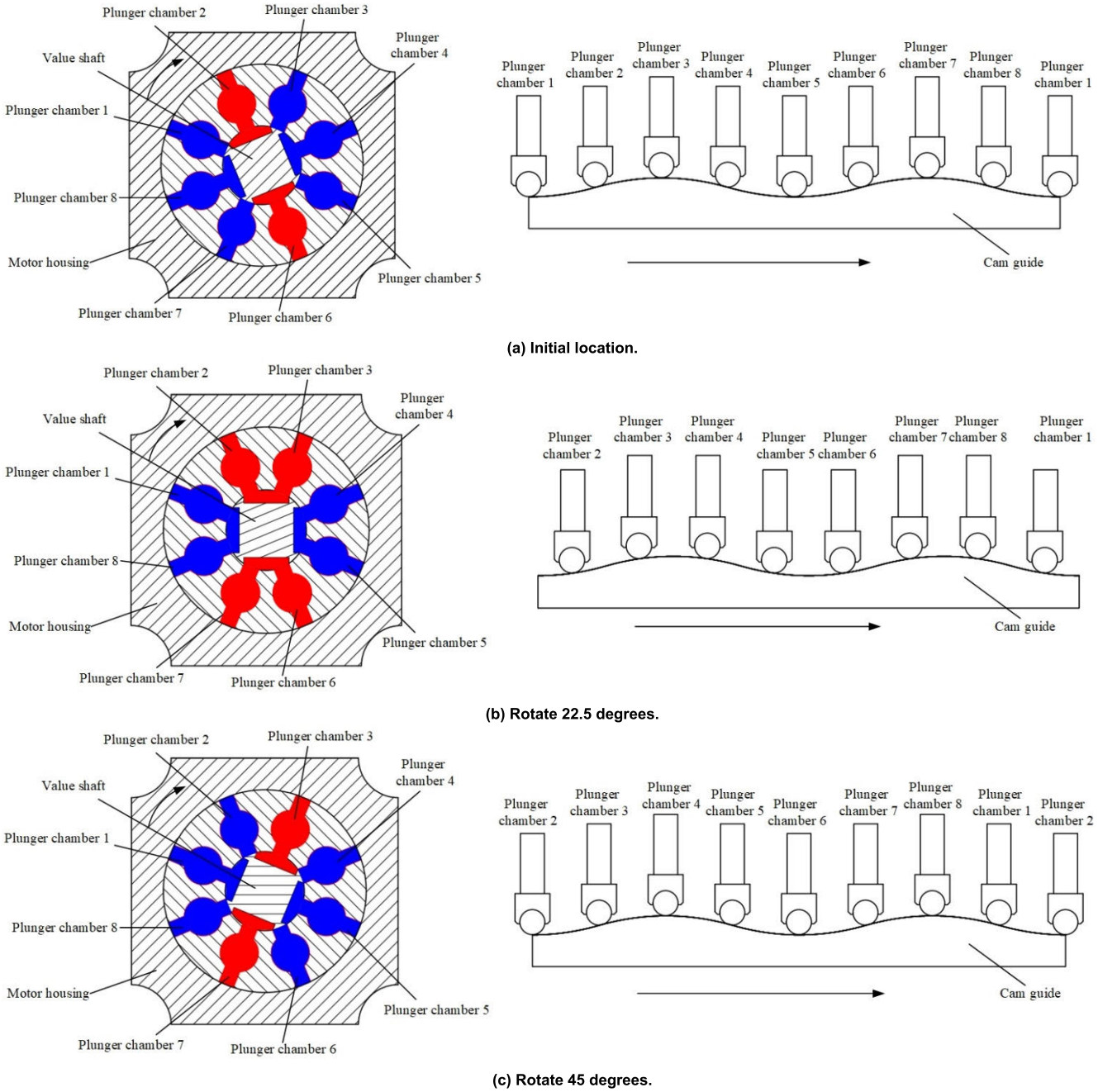

FIGURE 4. Schematic diagram of motor flow distribution state and plunger position.

cam shape on the flow distribution characteristics has been studied in the literature [13] and will not be expanded on in the paper.

Figure 5 shows a pair of plungers in the cylinder of the motor unit, and the bottom of the two plungers is a sealed pressure chamber, and the rollers on the outside of the plunger ends are in contact with the two cam surfaces, which are analytically modeled below to analyze the dynamic pressure of the plunger chamber.

The liquid flow from the pump output flows into or out of the plunger chamber through the flow distribution groove on the motor shaft and the flow distribution window on the cylinder block and is affected by the throttling effect, then the inflow and discharge flow rates of the i-th plunger chamber can be expressed as:

$$q_{ri,i} = C_d A_i \sqrt{\frac{2\,|p_{ci} - p_{in}|}{\rho}} sign(p_{ci} - p_{in}) \tag{1}$$

$$q_{ri,o} = C_d A_o \sqrt{\frac{2\,|p_{ci} - p_{case}|}{\rho}} sign(p_{ci} - p_{case}) \tag{2}$$

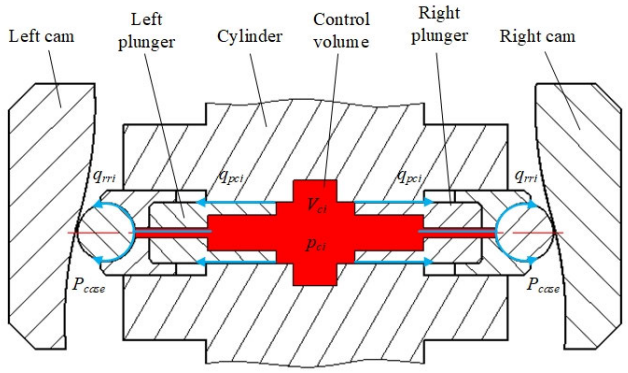

FIGURE 5. Schematic diagram of plunger chamber structure.

where C_d is the flow coefficient, P_{ci} is the dynamic pressure in the i-th plunger chamber, P_{in} is the motor inlet pressure, P_{case} is the case pressure, ρ is the density of water, A_i is the overflow area into the plunger chamber mating port, A_o is the outflow plunger chamber mating port outlet overflow area.

The change curves of inlet overflow area A_i and outlet overflow area A_o during the operation of the electro-hydraulic motor are shown in Figure 6.

Under the action of the cam normal force, the plunger is in an eccentric state in the cylinder bore and the resulting eccentric annular gap leakage can be expressed as:

$$q_{pci} = \frac{\pi d \delta_1^3 (p_{ci} - p_{case})}{12 \mu l_1}(1 + 1.5\varepsilon^2) + \frac{\pi d \delta_1 v_1}{2} \tag{3}$$

where d is the plunger diameter, δ_1 is the clearance between the plunger and the plunger chamber, μ is the dynamic viscosity of water, l_1 is the contact length between the plunger and the plunger cavity on the cylinder, ε is the relative eccentricity, v_1 is the plunger axial movement speed.

The hydrostatic support between the roller seat and the roller is stable, the thickness of the water film is balanced, and the liquid flow in the gap can be treated as the flow of a parallel plane gap with relative motion, the leakage can be expressed as:

$$q_{rri} = b\left(\frac{\delta_2^3 (p_{ci} - p_{case})}{12 \mu l_2} + \frac{v_2 \delta_2}{2}\right) \tag{4}$$

where b is the distance from the roller seat guide groove to the roller groove, δ_2 is the thickness of the water film between the roller and the roller seat, l_2 is the equivalent leakage length, v_2 is the sliding speed of the roller relative to the roller groove.

The plunger reciprocates in the plunger hole so that the plunger cavity confined volume changes instantaneously, and the fluid mass in the cavity can be expressed as:

$$M_{ci} = \rho V_{ci} \tag{5}$$

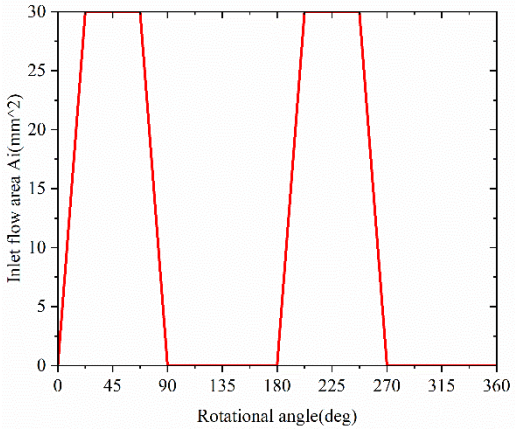

(a) Inlet overflow area A_i

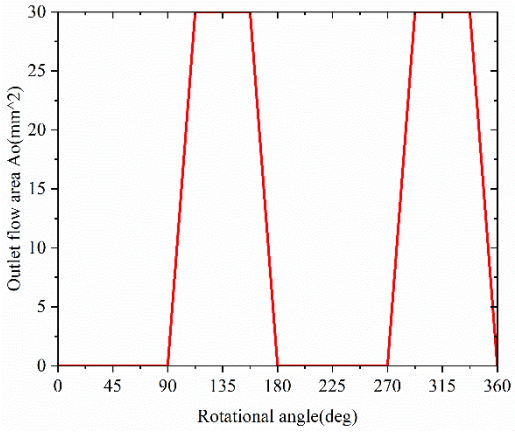

(b) Outlet overflow area A_o

FIGURE 6. Motor unit inlet and outlet overflow area change curve.

Then there can be expressed as:

$$\frac{dM_{ci}}{dt} = \frac{d\rho}{dt} V_{ci} + \rho \frac{dV_{ci}}{dt} \tag{6}$$

where V_{ci} is the transient volume of the plunger chamber.

Both plunger motion laws are the same, they jointly affect the change of plunger cavity volume, the transient volume of the plunger cavity can be expressed as:

$$V_{ci} = V_0 + 2 \cdot \frac{\pi d^2}{4} \cdot s_i \tag{7}$$

where V_0 is the minimum volume of the plunger chamber when the plunger is in the limit position, s_i is the displacement of the i-th plunger.

From the law of conservation of mass, the rate of change of the fluid mass in the plunger chamber can be expressed as:

$$\frac{dM_{ci}}{dt} = \rho q_{ci} \tag{8}$$

where q_{ci} is the volume flow rate into the plunger chamber.

$$\begin{cases} q_{ci} = q_{ri} - 2q_{pci} - 2q_{rri} \\ q_{ri} = q_{ri,i} + q_{ri,o} \end{cases} \tag{9}$$

where q_{ri} is the actual flow rate of fluid in the plunger chamber.

According to the defining equation for the bulk modulus of elasticity of a compressible fluid, it yields:

$$\frac{d\rho}{dt} = \frac{\rho}{K_e}\frac{dP_{ci}}{dt} \tag{10}$$

where K_e is the bulk modulus of elasticity of water.

Substituting equations (8) and (10) into equation (6), the dynamic pressure in the plunger chamber can be expressed as:

$$\begin{aligned}\frac{dP_{ci}}{dt} &= \frac{K_e}{V_{ci}}(q_{ri} - 2q_{pci} - 2q_{rri} - \frac{dV_{ci}}{dt}) \\ &= \frac{K_e}{V_0 + \frac{\pi d^2}{2}s_i}(q_{ri} - 2q_{pci} - 2q_{rri} - \frac{dV_{ci}}{dt})\end{aligned} \tag{11}$$

$$\begin{aligned}&q_{ri} - 2q_{pci} - 2q_{rri} - \frac{dV_{ci}}{dt} \\ &= C_d A_i\sqrt{\frac{2\left|p_{ci} - p_{in}\right|}{\rho}}sign(p_{ci} - p_{in}) \\ &\quad + C_d A_o\sqrt{\frac{2\left|p_{ci} - p_{case}\right|}{\rho}}sign(p_{ci} - p_{case}) \\ &\quad - \frac{\pi d\delta_1^3(p_{ci} - p_{case})}{6\mu l_1}(1 + 1.5\varepsilon^2) - \pi d\delta_1 v_1 \\ &\quad - \frac{b\delta_2^3(p_{ci} - p_{case})}{6\mu l_2} - bv_2\delta_2 \\ &\quad - \frac{d\left(V_0 + \frac{\pi d^2}{2}s_i\right)}{dt}\end{aligned} \tag{12}$$

Figure 7 shows the force on a plunger, which is modeled to analyze the output torque of the motor.

The hydraulic pressure to which the plunger is subjected can be expressed as:

$$F_{ci} = \frac{\pi}{4}d^2 P_{ci} \tag{13}$$

The inertial forces on the plunger assembly (including the rollers and roller seats) can be expressed as:

$$F_{ai} = ma_i \tag{14}$$

where m is the mass of the plunger assembly, a_i is the axial acceleration corresponding to the i-th plunger.

The cam and the roller are in the elastomeric fluid dynamic pressure lubrication state, and the simple algorithm proposed by Goksem [16] and Hargreaves [17] is used in this paper to calculate the rolling friction between the cam and the roller, and the friction between the cam and the roller in the elastomeric fluid dynamic pressure lubrication state is obtained as:

$$F_{EHD} = 29.2\frac{R_r}{\alpha}l_0(GU)^{0.648}W^{0.246} \tag{15}$$

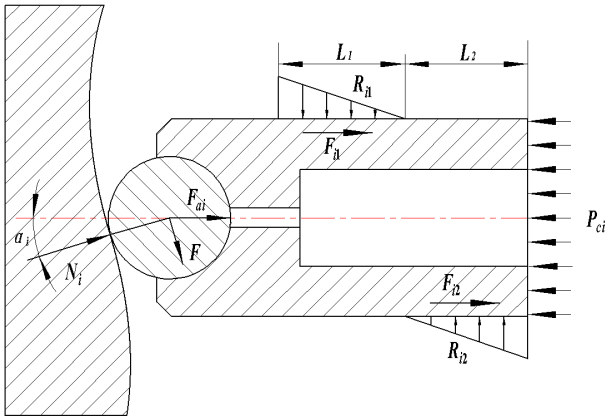

FIGURE 7. Sketch of force analysis of plunger.

where G is the dimensionless material parameter, U is the dimensionless velocity parameter, W is the dimensionless load parameter, R_r is the roller radius, l_0 is the roller length, α is the pressure-viscosity coefficient of water.

The rolling friction resistance between the roller and the cam is different at different positions, and the average value is taken after integration as:

$$F = \frac{\int_0^{2\pi} F_{EHD}d\theta}{2\pi} \tag{16}$$

Due to the positive pressure of the cam on the roller, contact stresses arise between the plunger and the cylinder bore, treating them equivalently as concentrated forces R_{i1} and R_{i2}, the frictional force between the plunger and the cylinder can be expressed as:

$$\begin{cases} F_{i1} = fR_{i1} \\ F_{i2} = fR_{i2} \end{cases} \tag{17}$$

where f is the coefficient of friction between the plunger and the cylinder block.

The force balance equation for the i-th plunger assembly in the horizontal direction can be expressed as:

$$F_{ci} - N_i\cos\alpha_i - (F_{i1} + F_{i2})sign\,(vi) + F\sin\alpha_i = ma_i \tag{18}$$

$$sign\,(vi) = \begin{cases} 1 & vi > 0 \\ 0 & vi = 0 \\ -1 & vi < 0 \end{cases} \tag{19}$$

where N_i is the support reaction force of the cam on the i-th plunger assembly, α_i is the pressure angle corresponding to the i-th plunger, v_i is the velocity corresponding to the i-th plunger.

The force balance equation for the i-th plunger assembly in the vertical direction can be expressed as:

$$N_i\sin\alpha_i + R_{i2} = F\cos\alpha_i + R_{i1} \tag{20}$$

From the triangular similarity principle of the force distribution, it follows:

$$\frac{R_{i1}}{R_{i2}} = \frac{L_1^2}{L_2^2} = k_t \tag{21}$$

From equations (18), (20) and (21), we can be expressed as:

$$R_{i1} = \frac{k_t[\sin\alpha_i(\frac{\pi}{4}d^2P_{ci} - ma_i) + F(\sin^2\alpha_i - \cos^2\alpha_i)]}{(k_t-1)\cos\alpha_i + (k_t+1)f\sin\alpha_i sign(vi)} \tag{22}$$

$$R_{i2} = \frac{\sin\alpha_i(\frac{\pi}{4}d^2P_{ci} - ma_i) + F(\sin^2\alpha_i - \cos^2\alpha_i)}{(k_t-1)\cos\alpha_i + (k_t+1)f\sin\alpha_i sign(vi)} \tag{23}$$

$$N_i = \frac{(k_t-1)(\frac{\pi}{4}d^2P_{ci} + F\sin\alpha_i - ma_i)}{(k_t-1)\cos\alpha_i + (k_t+1)f\sin\alpha_i sign(vi)} + \frac{(k_t+1)fF\cos\alpha_i sign(vi)}{(k_t-1)\cos\alpha_i + (k_t+1)f\sin\alpha_i sign(vi)} \tag{24}$$

As shown in Figure 4, the motor has two groups of 16 plungers, each group has 8 plunger assemblies, each group of 4 adjacent plungers and the other 4 have exactly the same law of action, the driving torque of the motor should be 4 times the output torque of the 4 adjacent plungers, so the driving torque produced by all the plungers acting together can be expressed as:

$$T_d = 4\sum_{i=1}^{4}(N_i\sin\alpha_i - F\cos\alpha_i)\cdot R_m = 4\sum_{i=1}^{4} \times \frac{(k_t-1)[\sin\alpha_i(\frac{\pi}{4}d^2P_{ci} - ma_i) + F(\sin^2\alpha_i - \cos^2\alpha_i)]}{(k_t-1)\cos\alpha_i + (k_t+1)f\sin\alpha_i sign(vi)}R_m \tag{25}$$

where R_m is the motor cam center diameter.

In equation (25), when the angle between the 1st plunger and the lowest point of the cam at moment t is θ, the corresponding angle of rotation of the i-th plunger at moment t is θ+(i-1)π/4, and the axial acceleration and corresponding pressure angle of the i-th plunger at moment t can be expressed as (26) and (27), shown at the bottom of the next page, where h is the plunger reciprocating stroke, ω is the angular velocity of the motor.

From this, the displacement of the i-th plunger in equation (7) is obtained as (28), shown at the bottom of the next page.

The axial force of the cam is borne by the thrust bearings on both sides, and the frictional resistance of the rolling bearing proposed in this paper with reference to the calculation method of the literature [18] can be expressed as:

$$T_f = T_0 + T_1 \tag{29}$$

$$T_0 = f_0(vn)^{2/3}d_m^3 \times 10^{-7} \tag{30}$$

$$T_1 = f_1F_ad_m \tag{31}$$

where T_0 is the component of friction moment related to the load size, lubricant, T_1 is with the load size, rolling body and raceway contact between the elastic deformation of the friction moment component, f_0 is the coefficient considering the bearing structure and lubrication method, d_m is the average diameter of the bearing, $d_m = (d_i + d_o)/2$, where d_i is the inner diameter of the bearing and d_o is the outer diameter of the bearing, v is the kinematic viscosity of water, n is the bearing speed, f_1 is the load factor, F_a is the axial load.

From the above analysis, the motor output torque can be expressed as:

$$T = T_d - T_f - J\frac{dw}{dt} \tag{32}$$

where J is the total rotational inertia on the motor shaft.

IV. SIMULATION MODEL

The imported motor unit model has to re-apply constraints to each part and add constraints to each part to limit its trajectory in conjunction with the actual working principle. In order to simulate the realistic motion of the motor, the actual loads on the motor are added, mainly the instantaneous fluid pressure on the bottom of the plunger, the Coulomb friction between the constrained components, and the contact force between the roller and the end cam.

After adding constraints, external loads, and internal loads to the geometric model of the motor unit, the dynamics simulation model of the motor unit is established, as shown in Figure 8.

The hydraulic model of the pump unit is created as a super element - the flow supply module - to provide flow to the hydraulic model of the motor unit, as shown in Figure 9.

The motor unit has 8 working chambers, each with 2 plunger assemblies on each side, and the motion of the 2 plunger assemblies together causes the pressure and flow rate changes in the volume chamber. The variation curve of the overflow area with rotation angle in Figure 6 is input to the dynamic_x_table sub-model of AMEsim to control the throttle opening. The throttle port is closed when the input signal is received as 0 and fully opened when the input signal is received as 1. The final model of the motor's single-group plunger working chamber is shown in Figure 10.

To realize the joint simulation, the Adams interface module needs to be added to the hydraulic model. The input variables of the Adams interface module are the hydraulic pressure applied to the 16 plungers, the output variables are the displacement and velocity of the 16 plungers, and the interface type is selected as AdamsCosim discrete mode. The hydraulic model of the 8 working chambers of the motor unit and the corresponding input and output of the Adams interface module is connected, and the flow is provided by the pump part super components to establish a joint

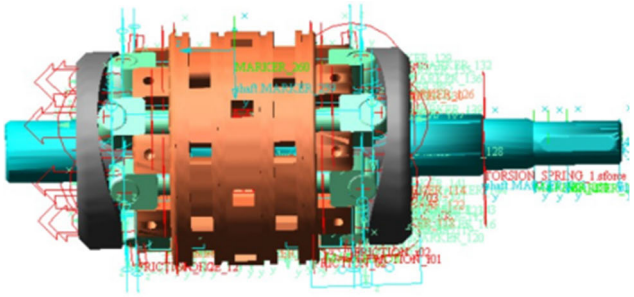

FIGURE 8. Motor unit core parts dynamics simulation model.

simulation model of the electro-hydraulic motor as shown in Figure 11.

The dynamics model of the motor unit mainly transmits the displacement and velocity of the plunger and the rotation angle of the motor shaft to the hydraulic model. The displacement and velocity of the plunger cause the working volume cavity of the plunger to change continuously, which affects the instantaneous hydraulic pressure change in the plunger cavity. The regularity of the working cavity of the plunger connected to the suction and discharge ports of the pump section is related to the rotation angle of the motor shaft.

V. ANALYSIS OF SIMULATION RESULTS

The electro-hydraulic motor joint simulation model is used to do a simulation analysis of its output characteristics, and the simulation parameters are shown in Table 1.

TABLE 1. Simulation Parameters.

Parameter	Value
Bulk modulus of the water K_e(MPa)	2180
Water viscosity μ(Pa·s)	1.01×10^{-3}
Water density ρ(kg/m^3)	1000
Tank pressure P_{case} (MPa)	0
Plunger diameter d(mm)	7.5
Chamber length at zero displacement	6
Plunger stroke h(mm)	6
The minimum volume of the plunger V_0(cm^3)	0.81
Flow coefficient C_d	0.62
The contact length between the plunger and the cylinder block	12.5

Since the working medium is water, the lubricity is poor, and the frictional wear increases when the plunger sub-gap is too small, which will cause the plunger to jam and reduce mechanical efficiency. Figure 12 shows the change curves of electro-hydraulic motor speed and single plunger sub-leakage when the plunger sub-gap is 5 μm, 8 μm, and 12 μm. It can be seen from the figure that with the increase of the plunger sub gap, the electro-hydraulic motor speed decreases, the average speed decreases from 730 r/min to 440 r/min, and the output speed decreases by 40%, and the speed pulsation also increases. Correspondingly, the internal leakage of the plunger sub increased sharply, as shown in Figure 13, from 0.012 L/min to about 0.3 L/min, an increase of 25 times. Since the contact length between the plunger

$$a_i = \begin{cases} \dfrac{16h\omega^2}{\pi^2}\theta + (i-1)\dfrac{\pi}{4} \in \left(k\pi \sim \dfrac{\pi}{4} + k\pi\right) \\ -\dfrac{16h\omega^2}{\pi^2}\theta + (i-1)\dfrac{\pi}{4} \in \left(\dfrac{\pi}{4} + k\pi \sim \dfrac{3\pi}{4} + k\pi\right) \\ \dfrac{16h\omega^2}{\pi^2}\theta + (i-1)\dfrac{\pi}{4} \in \left(\dfrac{3\pi}{4} + k\pi \sim \pi + k\pi\right) \end{cases} \tag{26}$$

$$\alpha_i = \begin{cases} \arctan\left(\dfrac{16h[\theta + (i-1)\frac{\pi}{4}]}{\pi^2 R_m}\right) \theta + (i-1)\dfrac{\pi}{4} \in \left(k\pi \sim \dfrac{\pi}{4} + k\pi\right) \\ \arctan\left(\dfrac{16h[\frac{\pi}{2} - (\theta + (i-1)\frac{\pi}{4})]}{\pi^2 R_m}\right) \theta + (i-1)\dfrac{\pi}{4} \in \left(\dfrac{\pi}{4} + k\pi \sim \dfrac{\pi}{2} + k\pi\right) \\ \arctan\left(\dfrac{16h[\theta + (i-1)\frac{\pi}{4} - \frac{\pi}{2}]}{\pi^2 R_m}\right) \theta + (i-1)\dfrac{\pi}{4} \in \left(\dfrac{\pi}{2} + k\pi \sim \dfrac{3\pi}{4} + k\pi\right) \\ \arctan\left(\dfrac{16h[\pi - (\theta + (i-1)\frac{\pi}{4})]}{\pi^2 R_m}\right) \theta + (i-1)\dfrac{\pi}{4} \in \left(\dfrac{3\pi}{4} + k\pi \sim \pi + k\pi\right) \end{cases} \tag{27}$$

$$s_i = \begin{cases} \dfrac{8h\left[\theta + (i-1)\frac{\pi}{4}\right]^2}{\pi^2} \theta + (i-1)\dfrac{\pi}{4} \in \left(k\pi \sim \dfrac{\pi}{4} + k\pi\right) \\ -\dfrac{8h\left[\theta + (i-1)\frac{\pi}{4}\right]^2}{\pi^2} + \dfrac{8h\left[\theta + (i-1)\frac{\pi}{4}\right]}{\pi} - h\,\theta + (i-1)\dfrac{\pi}{4} \in \left(\dfrac{\pi}{4} + k\pi \sim \dfrac{3\pi}{4} + k\pi\right) \\ \dfrac{8h\left[\theta + (i-1)\frac{\pi}{4}\right]^2}{\pi^2} - \dfrac{16h\left[\theta + (i-1)\frac{\pi}{4}\right]}{\pi} + 8h\theta + (i-1)\dfrac{\pi}{4} \in \left(\dfrac{3\pi}{4} + k\pi \sim \pi + k\pi\right) \end{cases} \tag{28}$$

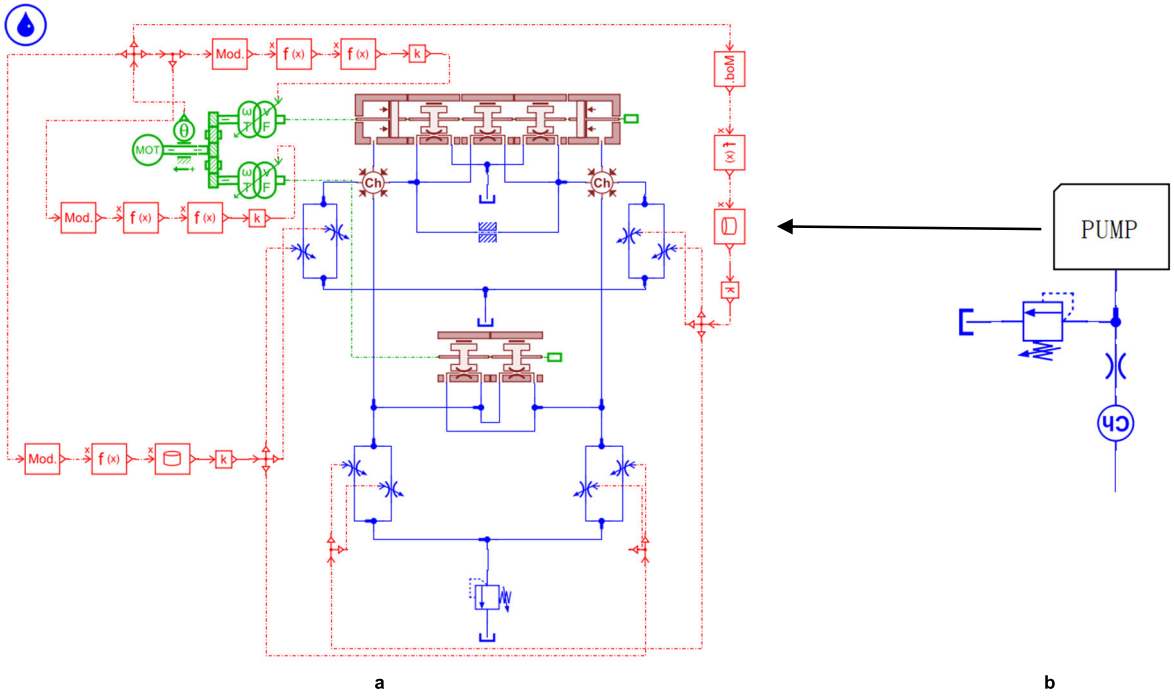

FIGURE 9. Hydraulic model of motor unit flow supply.

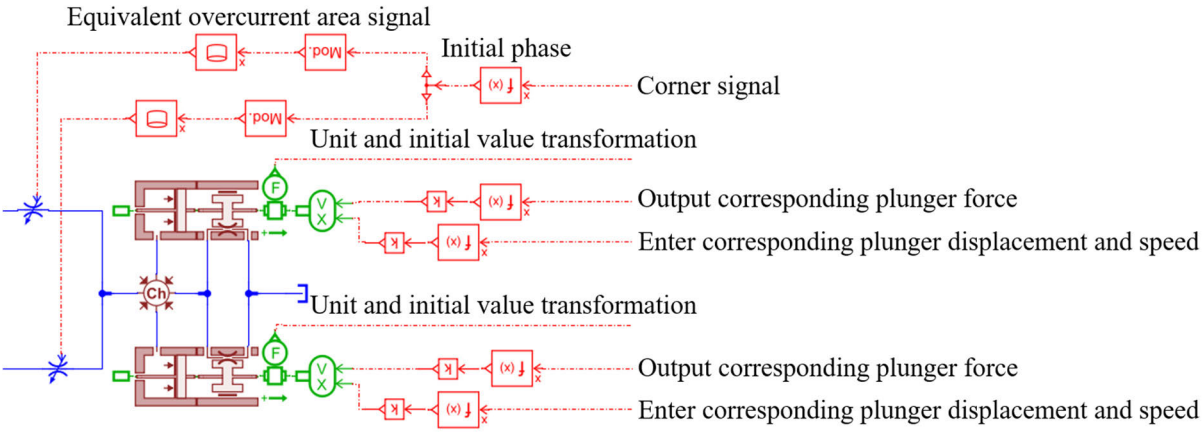

FIGURE 10. Single group plunger working volume cavity hydraulic model.

and the plunger bore varies when the plunger moves reciprocally in the plunger bore on the cylinder block, the plunger sub-leakage also varies. As the plunger sub-gap increases, the leakage volume increases, and the speed fluctuation increases.

Figure 14 shows the output speed curve of the electrohydraulic motor at different motor speeds. From the simulation curve, it can be seen that as the motor operating speed increases, the pump outlet flow rate increases, the response time of the electrohydraulic motor with load start becomes faster, and the motor output speed increases. The motor speed increases from 1000 r/min to 3000 r/min, and the pulsation amplitude of the electro-hydraulic motor speed decreases by 200%. It can be seen that as the motor speed increases, the pump outlet flow pulsation decreases, resulting in a significant improvement in the smoothness of the motor output speed.

Figure 15 shows the output speed curves of the electrohydraulic motor when the outlet pressure (back pressure) of the motor unit is 0.2 MPa, 0.7 MPa, and 1.2 MPa. From the simulation results, it can be seen that with the increase of the motor outlet pressure, the fluctuation of the rotational speed at the beginning of the electrohydraulic motor start-up

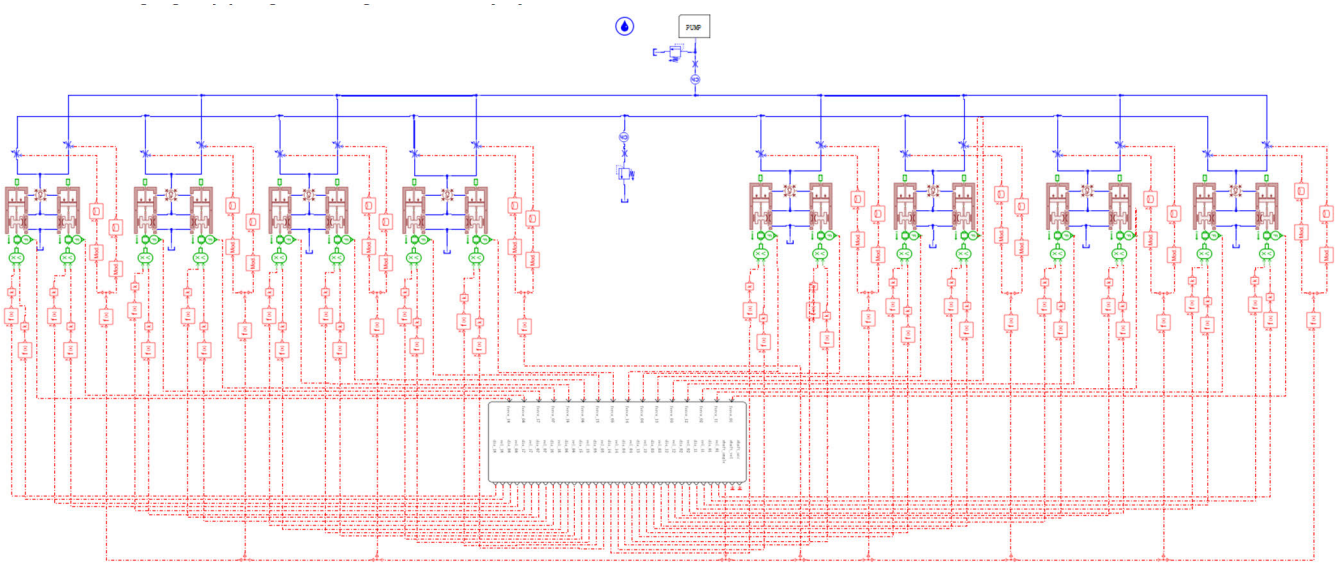

FIGURE 11. Electro-hydraulic motor joint simulation model.

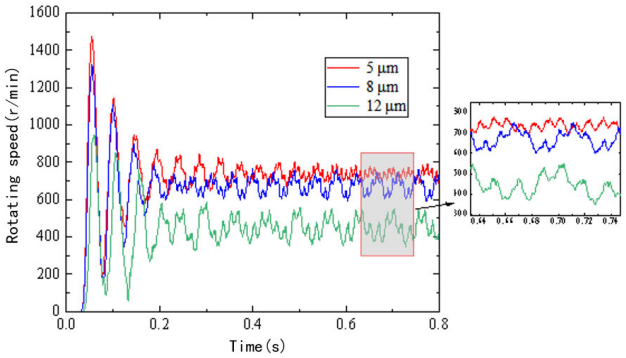

FIGURE 12. Effect of plunger sub clearance on the speed of electrohydraulic motor.

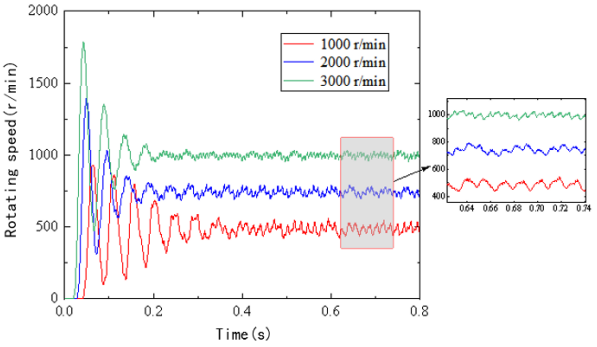

FIGURE 14. Relationship between motor speed and electro-hydraulic motor output speed.

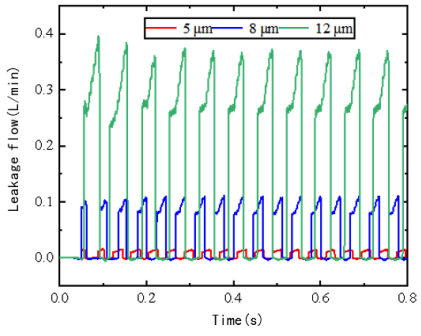

FIGURE 13. Effect of plunger sub gap on plunger sub leakage.

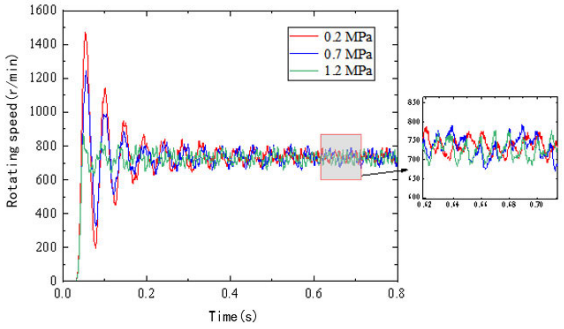

FIGURE 15. Effect of back pressure on the speed of electrohydraulic motor.

decreases significantly, but the magnitude and the mean value of the rotational speed fluctuation remain the same after the stabilization. Therefore, the back pressure of the motor can be increased appropriately by adding a check valve at the motor inlet and outlet, which can prevent the large sudden change of the rotational speed during the electrohydraulic motor start-up.

The motor output torque is proportional to the motor inlet and outlet pressure difference, driving the same load, the inlet pressure will also increase due to the increase of back

TABLE 2. Table of formulate.

Symbol	Unit	Description
C_d	[-]	flow coefficient
P_{ci}	[MPa]	the dynamic pressure in the i-th plunger chamber
P_{in}	[MPa]	the motor inlet pressure
P_{case}	[MPa]	the case pressure
ρ	[g/mm3]	the density of water
A_i	[mm2]	the overflow area into the plunger chamber mating port
A_o	[mm2]	the outflow plunger chamber mating port outlet overflow area
d	[mm]	the plunger diameter
δ_1	[mm]	the clearance between the plunger and the plunger chamber
μ	[Pa/s]	the dynamic viscosity of water
l_1	[mm]	the contact length between the plunger and the plunger cavity on the cylinder
ε		the relative eccentricity
v_1	[mm/s]	the plunger axial movement speed
b	[mm]	the distance from the roller seat guide groove to the roller groove
δ_2	[mm]	the thickness of the water film between the roller and the roller seat
l_2	[mm]	the equivalent leakage length
v_2	[mm/s]	the sliding speed of the roller relative to the roller groove
V_{ci}	[mm3]	the transient volume of the plunger chamber
V_0	[mm3]	the minimum volume of the plunger chamber when the plunger is in the limit position
s_i	[mm]	the displacement of the i-th plunger
q_{ci}	[mm3/s]	the volume flow rate into the plunger chamber
q_{ri}	[mm3/s]	the actual flow rate of fluid in the plunger chamber
K_e	[MPa]	the bulk modulus of elasticity of water
m	[Kg]	the mass of the plunger assembly
a_i	[m/s2]	the axial acceleration corresponding to the i-th plunger
G	[-]	the dimensionless material parameter
U	[-]	the dimensionless velocity parameter
W	[-]	the dimensionless load parameter
R_r	[m]	the roller radius
l_0	[m]	the roller length
α	[m2/N]	the pressure-viscosity coefficient of water
f	[-]	the coefficient of friction between the plunger and the cylinder block
N_i	[N]	the support reaction force of the cam on the i-th plunger assembly
α_i	[-]	the pressure angle corresponding to the i-th plunger
v_i	[mm/s]	the velocity corresponding to the i-th plunger

TABLE 3. *(Continued.)* Table of formulate.

R_m	[mm]	the motor cam center diameter
h	[mm]	the plunger reciprocating stroke
ω	[rad/s2]	the angular velocity of the motor
T_0	[Nm]	the component of friction moment related to the load size
T_1	[Nm]	with the load size, rolling body and raceway contact between the elastic deformation of the friction moment component
f_0	[-]	the coefficient considering the bearing structure and lubrication method
d_m	[mm]	the average diameter of the bearing
d_i	[mm]	the inner diameter of the bearing
d_o	[mm]	the outer diameter of the bearing
v	[mm2/s]	the kinematic viscosity of water
n	[r/min]	the bearing speed
f_1	[-]	the load factor
F_a	[N]	the axial load
J	[kg/m2]	the total rotational inertia on the motor shaft

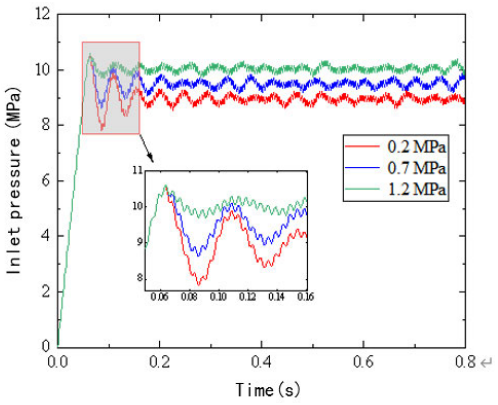

FIGURE 16. Effect of back pressure on motor inlet pressure.

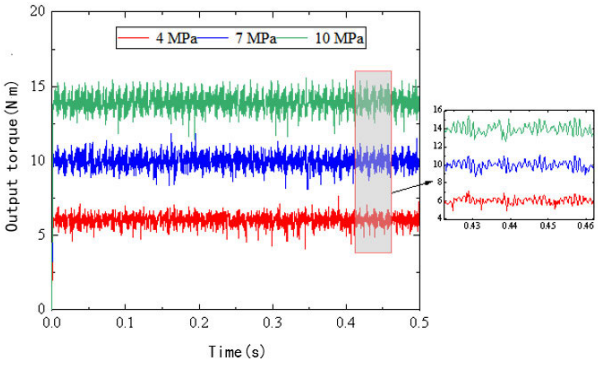

FIGURE 17. Output torque characteristics of electro-hydraulic motor and its relationship with inlet and outlet pressure difference.

pressure. Figure 16 shows the motor inlet pressure curves corresponding to different back pressure values. As can be seen from the figure, the back pressure value increases from 0.2 MPa to 1.2 MPa, the motor inlet pressure increases from 9 MPa to 10 MPa, and the pressure pulsation at the beginning

of the start-up period is also reduced significantly. It can be seen that the appropriate back pressure can reduce the speed and inlet pressure pulsation, which is conducive to the smooth operation of the electro-hydraulic motor and less shock and vibration. However, the back pressure also makes the system pressure rise, resulting in increased leakage, and the back pressure also makes the frictional wear of the drain chamber plunger increase, all of which will make the efficiency decrease.

As shown in Figure 17, the output torque of the electrohydraulic motor varies in accordance with a certain periodic period of 0.01 s at a certain speed, and the corresponding motor rotation angle is $\pi/4$. When the output speed is 780 r/min and the differential pressure between the inlet and outlet is 4 MPa, 7 MPa, and 10 MPa, the corresponding output torque of the electrohydraulic motor is about 6 Nm, 10 Nm, and 14 Nm, and the differential pressure between inlet and outlet increases by 2.5 times and the output torque increased by 2.3 times accordingly.

VI. CONCLUSION

(1) A new integrated water-hydraulic electrohydraulic motor mechanical structure designed with a two-dimensional hydraulic component design principle is proposed in this paper, whose unique design is to realize the two-dimensional motion of the pump unit piston and the axial reciprocating motion of the motor unit plunger by using the end cam mechanism. Among them, the pump unit is designed with an oil-water separation structure to improve the transmission efficiency and life, and the motor unit is designed with two sets of the plunger and cam mechanism to achieve the balance of axial force and make the output characteristics more stable.

(2) Compared with the traditional water-hydraulic motor, the integrated electro-hydraulic motor does not need an external power source, and the weight of the body is only 4.8 Kg, which is lighter than the traditional swashplate water-hydraulic motor (which also needs an additional power source). The electro-hydraulic motor can achieve a wide range of speed regulation through the motor so that the electro-hydraulic motor has a large range of working speeds; while the traditional swashplate water-hydraulic motor can only be regulated by valve control, which makes the working efficiency lower.

(3) The results show that the plunger sub has a great influence on the speed, and the motor unit should be selected with proper clearance. The motor speed increase can significantly improve the speed smoothness, and the pulsation amplitude of the electro-hydraulic motor speed is reduced by 200% when the motor speed is increased from 1000 r/min to 3000 r/min. Proper back pressure can effectively prevent the large sudden change of speed during the start of an electro-hydraulic motor, which is conducive to the smoothness of electro-hydraulic motor operation and less shock and vibration. The output torque of the electrohydraulic motor changes periodically according to a certain rule, with a period of 0.01 s, corresponding to a motor rotation angle of $\pi/4$. Therefore, the structure and working parameters of the electrohydraulic motor can be selected as follows: the plunger sub-gap is selected according to 8 μm; the back pressure is taken at 0.5∼0.8 MPa; the motor speed needs to exceed 3000 r/min. In order to realize the back pressure of the motor, four check valves need to be added to the motor outlet.

REFERENCES

[1] Y. S. Liu, D. F. Wu, D. L. Li, X. F. Zhao, and X. H. Li, "Applications of seawater hydraulics in deep-sea equipment," *J. Mech. Eng.*, vol. 50, no. 2, pp. 28–35, Jan. 2014, doi: 10.3901/JME.2014.02.028.

[2] Y. S. Liu, Z. J. Guo, B. H. Zhu, X. F. He, and Z. Y. Li, "Underwater tool system driven by seawater hydraulic power," *Ocean Technol.*, vol. 25, no. 4, pp. 65–69, Dec. 2006.

[3] S. D. Yang, Z. Y. Li, Z. Y. Yu, and Y. Q. Zhu, "Seawater hydraulic powered underwater operation tools," *Ocean Technol.*, vol. 17, no. 2, pp. 50–55, Jun. 1998.

[4] X. F. He, Q. G. Huang, B. H. Zhu, S. Y. Liu, and Z. Y. Li, "A seawater hydraulic diver tool system," *Chin. Hydraul. Pneum.*, vol. 8, pp. 49–51, Feb. 2004.

[5] N. D. Manring and S. B. Kasaragadda, "The theoretical flow ripple of an external gear pump," *J. Dyn. Syst., Meas., Control*, vol. 125, no. 3, pp. 396–404, Sep. 2003.

[6] N. D. Manring, V. S. Mehta, B. E. Nelson, K. J. Graf, and J. L. Kuehn, "Scaling the speed limitations for axial-piston swash-plate type hydrostatic machines," *J. Dyn. Syst., Meas., Control*, vol. 136, no. 3, May 2014, doi: 10.1115/1.4026129

[7] K. Matsumoto and M. Ikeya, "Friction and leakage characteristics between the slipper and swashplae for starting and low-speed conditions in a swashplate-type axial piston motor," *Trans. Jpn. Soc. Mech. Eng. C*, vol. 57, no. 541, pp. 3013–3018, 1991.

[8] M. C. Ke, F. Ding, B. Li, and Z. G. Chen, "Exploration of the influence of backing pressure on the efficiency of hydraulic motor," *Trans. Chin. Soc. Agricult. Machinery*, vol. 37, no. 10, pp. 127–131, Oct. 2006.

[9] D. S. Wen, L. J. Sun, B. Xi, F. Du, D. X. Li, and G. Q. Zhao, "Output torque characteristics analysis of double swash plate multi-row axial piston motor," *Trans. Chin. Soc. Agricult. Machinery*, vol. 51, no. 6, pp. 420–426, Jun. 2020, doi: 10.6041/j.issn.1000-1298.2020.06.046.

[10] L. J. Yang, S. L. Nie, S. Yin, and L. Wang, "Simulation based on virtual prototype modeling for output characteristics of seawater piston motor," *Chin. Hydraul. Pneum.*, no. 7, pp. 28–30, 2015, doi: 10.11832/j.issn.1000-4858.2015.07.006.

[11] L. Yang, S. Nie, S. Yin, J. Zhao, and F. Yin, "Numerical and experimental investigation on torque characteristics of seawater hydraulic axial piston motor for underwater tool system," *Ocean Eng.*, vol. 104, pp. 168–184, Aug. 2015, doi: 10.1016/j.oceaneng.2015.05.003.

[12] D. C. Jin and J. Ruan, "Design and research of two-dimensional fuel pump," *Acta Aeronautica Astronautica Sinica*, vol. 40, no. 5, p. 12, May 2019, doi: 10.7527/S10006-893.2019.22730.

[13] D. C. Jin, J. Ruan, T. Xing, and L. F. Wang, "Design and experiment of two-dimensional cartridge water pump based on mathematical model," *Trans. Chin. Soc. Agricult. Machinery*, vol. 50, no. 7, pp. 177–185, Jul. 2019, doi: 10.6041/j.issn.1000-1298.2019.07.018.

[14] J. Y. Qian, S. N. Shentu, and J. Ruan, "Volumetric efficiency analysis of two-dimensional piston aviation fuel pump," *Acta Aeronautica Astronautica Sinica*, vol. 41, no. 4, p. 13, Apr. 2020, doi: 10.7527/S10006-893.2019.23267.

[15] S. N. Shentu, J. Ruan, J. Y. Qian, and B. Meng, "Optimization analysis of flow characteristic and distribution window of 2D pump," *Trans. Chin. Soc. Agricult. Machinery*, vol. 50, no. 12, pp. 403–410, Dec. 2019, doi: 10.6041/j.issn.1000-1298.2019.12.047.

[16] P. G. Goksem and R. A. Hargreaves, "The effect of viscous shear heating on both film thickness and rolling traction in an EHL line contact—Part I: Fully flooded conditions," *J. Lubrication Technol.*, vol. 100, no. 3, pp. 346–352, Jul. 1978.
[17] P. G. Goksem and R. A. Hargreaves, "The effect of viscous shear heating on both film thickness and rolling traction in an EHL line contact—Part II: Starved conditions," *J. Lubrication Technol.*, vol. 100, no. 3, pp. 353–358, Jul. 1978.
[18] A. H. Zhu, C. J. Zhu, and W. H. Zhuang, "Analysison calculation of friction torque of rolling bearings," *Bearing*, no. 7, p. 3, 2008, doi: 10.19533/j.issn1000-3762.2008.07.001.

TONG XING received the Ph.D. degree in mechanical-electronic-engineering from Zhejiang University, China, in 2008. From 2013 to 2014, he was a Visiting Scholar, he made researches on the characteristics of hydraulic pumps with the Maha Research Center, Purdue University, USA. He is currently an Associate Professor with the School of Mechanical Engineering, Zhejiang University of Technology, China. His research interests include electro-hydraulic servo control systems and components.

YING HUANG is currently pursuing the degree with the 2D Hydraulic/Pneumatic Components and Systems Engineering Technology Research Center, School of Mechanical Engineering, Zhejiang University of Technology. Her research interests include electro-hydraulic control components and systems.

CUN GAO is currently pursuing the degree with the 2D Hydraulic/Pneumatic Components and Systems Engineering Technology Research Center, School of Mechanical Engineering, Zhejiang University of Technology. His research interests include electro-hydraulic control components and systems.

JIAN RUAN received the Ph.D. degree from the Harbin Institute of Technology. He is currently a Professor, a Doctoral Tutor, and the Director of the 2D Hydraulic/Pneumatic Components and Systems Engineering Technology Research Center, School of Mechanical Engineering, Zhejiang University of Technology. His research interests include electro-hydraulic digital control systems and components, and electromechanical control technology.